Experiment 6/7:
Harmonic Oscillator: Physical Pendulum and Waves on a Vibrating String

Samiha Rahman
UID: 404792929
Date of Experiment: August 28 – September 6, 2017
Lab Section: Monday/Wednesday, 11:30 AM
TA: Nicholas Rombes III
Lab Partner: Rafi Hessami
Abstract Word Count: 162

Examining harmonic motion in single-point and spatially extensive systems

S. Rahman[1]

Harmonic motion can be exhibited by rigid and non-rigid, spatially extensive systems; the behavior for each type of system is characterized in this experiment. The harmonic oscillations of a physical aluminum pendulum were damped by controlling its proximity to a set of magnets. This allowed for observation of its underdamped, overdamped, and critically damped regimes. Then the resonant frequency of the driven damped oscillations, found by plotting Lissajous figure, was measured to be $(0.875 \pm 0.025)s^{-1}$. The harmonic motion of a vibrating string was also observed by relating the string's tension to the speed of its travelling waves. Despite the inconsistency between the predicted and measured speed, the positive correlation between tension and speed is confirmed. The fundamental frequency of the standing waves produced by the string was determined to be $(10.67 \pm 0.05)s^{-1}$, which was used to locate the successive harmonics. Finally, the constraint of the middle node was found to only affect the modes that did not have a node at the controlled position.

[1] *Department of Computer Science, University of California, Los Angeles*

INTRODUCTION

Harmonic motion of a system is defined as its periodic displacement relative to an equilibrium point. While this phenomenon is generally associated with rigid systems, such behavior can be exhibited by non-rigid systems. The components affecting the harmonic motion of each system are therefore investigated in this experiment.

In a rigid body, the displacement is localized at a single point. This is demonstrated by an aluminum anchor-shaped pendulum as it oscillates between a set of magnets. Adjustment of the magnet spacing allow for a controlled examination of the three damping regimes: underdamped (displacement changes sign at least once), overdamped (displacement does not change sign), and critically damped (crossover between regimes). The resonant frequency of the damped oscillations is also found through controlling the pendulum's oscillations with a wave driver. This is measured using Lissajous figures that plot angular displacement vs. output voltage data. A graph relating the amplitude of different driving frequencies is produced to analyze what is the system's resonance.

To then observe a non-rigid, spatially extensive system where there is no localized point, a string is vibrated using a wave driver to produce travelling waves. This motion is tracked using a laser beam, which scatters into a photodiode. Different tensions are applied to the string to experimentally confirm that a string's tension and linear mass density affects its speed. Standing waves are then produced with the same setup by finding the resonant frequency for the fundamental mode n = 1 with the Lissajous figures method. This measurement is used to predict the harmonics that follow. Finally, the effects of intermediate boundary conditions are observed by constraining the middle node for multiple modes.

METHODS

Harmonic Oscillations in Physical Pendulum

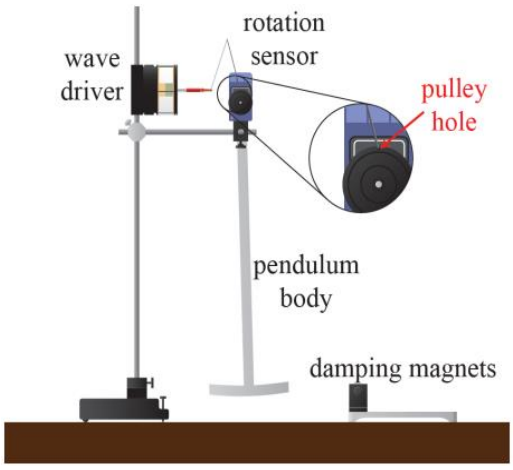

Figure 1. Setup for Physical Pendulum. Figure reproduced (with permission) from Fig. 6.1 by Campbell, W. C. et al. Physics 4AL: Mechanics Lab Manual (ver. May 12, 2017). (Univ. California Los Angeles, Los Angeles, California).

To set up the equipment as is shown in Figure 1, the spring on the wave drive is connected to the wheel of the rotation sensor by putting the V-shaped torsion spring through the hole of the pulley. The system is elevated using rods and clamps and set at a height so that the

pendulum body can swing freely but is centered at the level of the damping magnets. The equilibrium position of the resting pendulum is zeroed by clicking "Zero Sensor Now" in the rotary motion sensor settings on Capstone. As a precaution to decrease uncertainty, this is done before each trial.

Part 1: Harmonic motion with damping

To start an oscillation, the pendulum is displaced slightly from its equilibrium point. This initial displacement of the pendulum is kept constant for each trial using a photogate sensor as a reference point (i.e. the pendulum unblocks the sensor immediately after it is released). The pendulum is released and is allowed to swing freely for at least 5-10 seconds. During this run, the angular displacement vs. time data is recorded in a table and is displayed on a graph in Capstone, where the damping regime can be determined (with an appropriate sampling rate).

After an initial trial without the magnets is run, the damping is controlled by adjusting the spacing of the magnets through which the pendulum swings. The spacing between the magnets is changed for each trial, varying between the maximum and minimum gap, for a total of five trials. These trials are used to narrow down and determine the spacing for which the damping is critically damped. The gaps are changed with ~1 mm steps until the fastest damping is seen on the graph.

Part 2: Harmonic motion with driving

Before driving the oscillations, the spacing of the magnets is set constant so that the oscillations damp out within 5-10 seconds; the angular displacement vs. time data is recorded for this setup in undriven conditions. A graph is added on Capstone to display the angle on the y-axis and driver voltage on the x-axis (this parametric plot is called a Lissajous figure). The oscillations are powered by the wave driver using the "Signal Generator" function on Capstone, with which the amplitude is set below 5 V and the frequency can be adjusted. The frequency is adjusted until the resonant frequency is found; this is defined to be when the Lissajous figure is a horizontal ellipse (the ellipse is tilted at other frequencies). The uncertainty bounds of this measurement are estimated by decreasing and increasing the frequency from $\omega_{R_{measured}}$ until the produced graph is distinguishable from the horizontal ellipse.

The angle vs. voltage data is then recorded for 10 different drive frequencies that are below, at, or above the resonant frequencies. A few frequencies are chosen within $\pm 0.02\ s^{-1}$ of $\omega_{R_{measured}}$, and others are chosen to be at least $0.1\ s^{-1}$ from $\omega_{R_{measured}}$.

Waves on a Vibrating String

Figure 2. Setup for Vibrating String. A rod holds the photodiode and laser device. Figure reproduced (with permission) from Fig. 7.1.a by Campbell, W. C. et al. Physics 4AL: Mechanics Lab Manual (ver. May 12, 2017). (Univ. California Los Angeles, Los Angeles, California).

As shown in Figure 2, two rods are clamped down about a meter apart. A string is tightly attached to both ends. On the left, it is attached using a clip clamp, with the wave driver's

actuator tip, positioned 1-2 mm from the clamp, just barely touching the string. On the right, it is placed on a pulley with a hanging weight at the end to provide tension. On a standing rod, a laser device is set up 6-8 cm from the pulley apex so that its horizontal laser beam covers about a top third of the string. The photodiode is set directly above the beam spot with a gain setting of 10.

Part 1: Wave Speed

This part compares the predicted and experiment values of the wave speed, which depend on tension and linear mass density. Since the tension of the string varies by the hanging mass, the following measurements are taken in the respective order: mass of the hanging weight, total mass of the string, total length of the relaxed unattached string, length of the excess string beyond the clamp, total length of the stretched string (from clip clamp to knot on hanging weight), and length of hanging portion of string. The length between the pulley and the clamp is measured for the experimental calculation as well. Since each trial has a different hanging weight, the mass of the hanging weight and the length of the stretched string—total and hanging—will change and must be measured each time. These are used to measure the tension and linear mass density of the string.

Three trials are done with different hanging weights, with one being at least 350 grams. The wave driver is controlled in the Signal Generator function of Capstone, where the constant settings used are: Waveform= Square, Frequency=0.250 Hz, and Amplitude = 1.0 V. The Light Intensity (%) and Output Voltage (V) data are recorded versus time on a table and visualized on a Graph.

Part 2: Standing Waves

To produce the best results for the standing waves, the heaviest hanging weight is used on the string. Using the Signal Generator, the resonant frequency is found for the fundamental mode (n=1) by changing the frequency and observing the amplitude. The frequency, measured to the hundredth, is recorded to be the resonant frequency when the amplitude shown is highest.

A second method of finding the resonant frequency is by looking for symmetric Lissajous figures of the light intensity vs. voltage data. The resonant frequency is recorded (ideally equivalent to the frequency found earlier) and is used to predict the resonant frequencies for the following harmonics n =2, 3, 4, 5, 6, 7, 8 and 9. These predictions are then adjusted to produce a symmetric Lissajous figure to measure the actual resonant frequency at the mode. The uncertainty is estimating by seeing how much of a deviation from the resonant frequency will cause the Lissajous ellipse to no longer be symmetric. The amplitude is increased as needed to produce clear signals. The same procedure is attempted for n = 30 and ideally up to n = 60.

Part 3: Boundary Effects

To investigate intermediate boundary conditions and interference, the string is driven at a constant amplitude at the measured resonant frequencies for n=2, 4, and 5. The peak-to-peak size of the photodiode signal is recorded as the “amplitude” for each mode. Then, for each mode a ring stand and post is used to constrain the mode at the middle node on the string and the new amplitude for the mode is recorded. The post is in the same position for each mode.

ANALYSIS

Harmonic Oscillations in Physical Pendulum

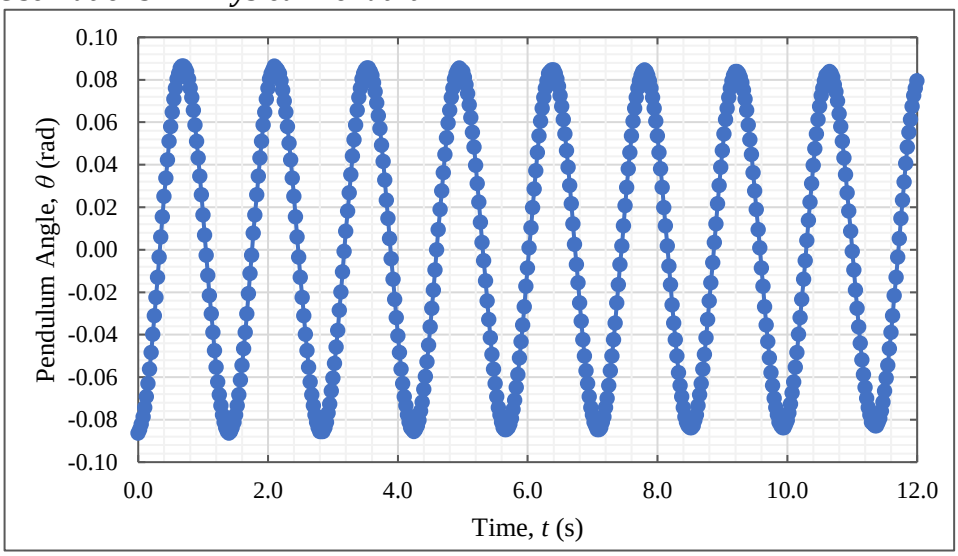

Figure 3. Undamped Oscillation of Physical Pendulum. The pendulum was released at a small displacement from $\theta = 0$, since the theory assumes small angle approximation ($sin(\theta) \approx \theta$, $cos(\theta) \approx 1$). The magnets are temporarily removed from the setup to ensure no external damping force affected the oscillations. While the zero measurement was set to the equilibrium point, a vertical offset was still required to center the oscillations at 0 radians. This was done by subtracting the data by the average midpoint of the maximum and minimum peaks.

To find the undamped oscillation frequency, the time for each peak is found on Excel by approximating the time point on the graph and then locating the exact time of the maximum within the data. The average frequency at each peak (from the 1st peak to the nth peak) was found using the formula $\omega_{o_{avg}} = \frac{n-1}{t_n - t_1}$. The best value for ω_o was taken to be the average of all calculated frequencies, and the error is estimated by systematic uncertainty $\delta\omega_o = \frac{STDEV.S\left(All\ \omega_{o_{avg}}\right)}{\sqrt{7}}$. This gives $\omega_o = (0.7067 \pm 0.0014)\text{s}^{-1}$.

Part 1: Harmonic Motion with Damping

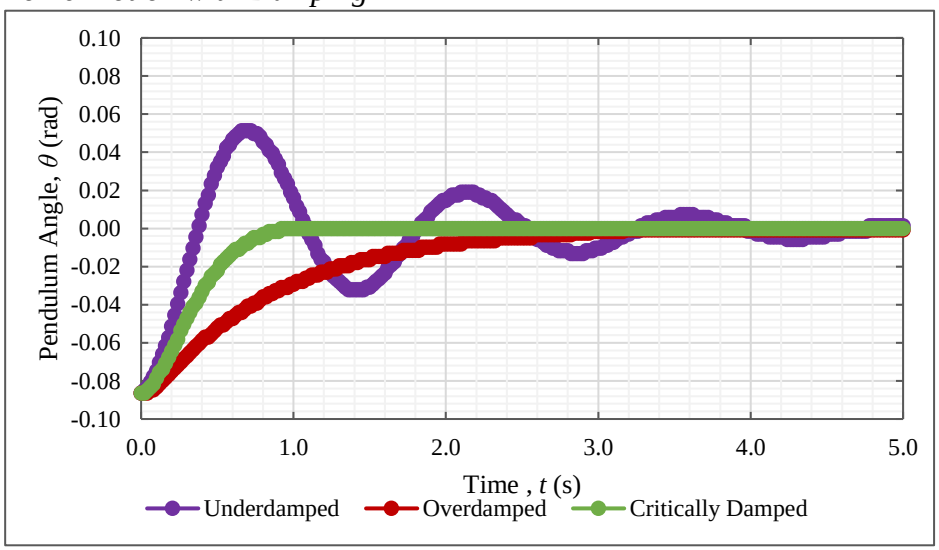

Figure 4. Damping Regimes of Pendulum Oscillator. The underdamped oscillation above was produced by a magnet spacing of $(24.61 \pm 0.05)\ mm$. As can be seen, the oscillation never reaches the original displacement due to damping but a few cycles are still produced. The overdamped oscillation was produced by a magnet spacing of $(9.23 \pm 0.05)\ mm$. The strong damping force causes the displacement to not change sign, but it takes a while to reach the equilibrium point. Steps of ~1mm were then taken from the overdamped oscillation spacing to find the spacing that produced a critically damped oscillation, where the oscillation damps out the fastest. This was determined to be $(14.1 \pm 0.3)mm$. The uncertainty is estimated by the lack of precise adjustment for the magnet spacing.

The damping constants that produce oscillations in each regime can be described in relationship to the undamped frequency $\omega_o = (0.7067 \pm 0.0014)\mathrm{s}^{-1}$:

- Underdamped motion is achieved when $\omega_o > \frac{1}{\tau}$. For such motion, ω_{damped} is real since the period of at least one cycle can be estimated if at least half of a cycle exists; this is consistent with the requirement that displacement changes sign as least once. Therefore, for this system, the minimum damping constant can be described by

$$(0.7067 \pm 0.0014)\mathrm{s}^{-1} > \frac{1}{\tau}$$

$$\tau > \left((0.7067 \pm 0.0014)\mathrm{s}^{-1}\right)^{-1}, \delta\tau = |-1| * \frac{0.0014}{0.7067^2}$$

$$\tau > (1.415 \pm 0.003)s$$

- Overdamped motion is achieved when $\omega_o < \frac{1}{\tau}$. Since the oscillation is completely damped out by the time displacement returns to the equilibrium point, ω_{damped} cannot be measured and is thus imaginary. Such behavior occurs when the damping constant is below the maximum value defined by $\tau < \frac{1}{\omega_o}$, which is $\tau < (1.415 \pm 0.003)s$. Note that the value can be obtained from the previous computation as the guidelines both involve $\frac{1}{\omega_o}$.

- Critically damped motion is achieved when $\omega_o = \frac{1}{\tau}$, or $\tau = (1.415 \pm 0.003)s$. The damping force is strong enough to damp out the oscillation by the time it reaches the displacement; however, the force still allows the motion to reach the equilibrium point relative quickly. This behavior demonstrates the crossover between underdamped and overdamped oscillation.

Part 2: Harmonic Motion with Driving

The resonant frequency of the damped oscillation is then found using the wave driver. Before measuring this however, the resonant frequency can be predicted using the formula $\omega_R = \sqrt{\omega_o^2 - 2\frac{1}{\tau^2}}$. The undamped frequency was determined in Part 1 to be $\omega_o = (0.7067 \pm 0.0014)\text{s}^{-1}$. Therefore, the damping constant τ must be found for the constant setup used, where the magnets are spaced (25.22 ± 0.05)mm apart.

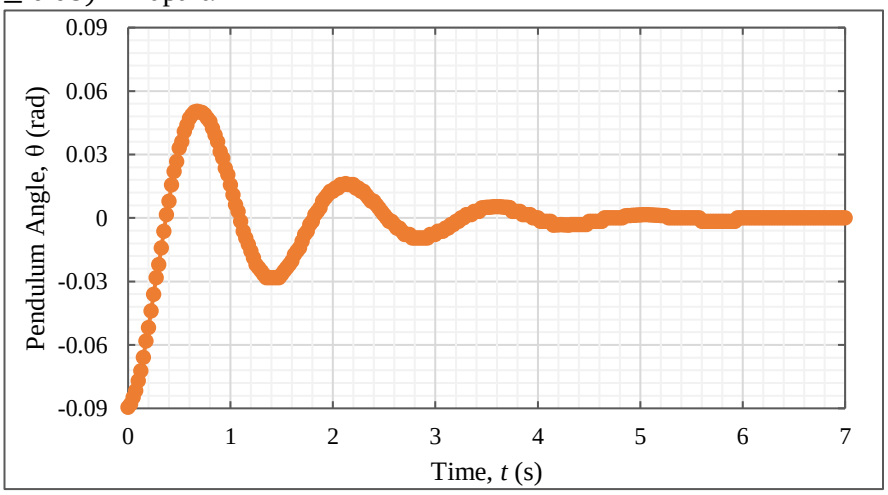

Figure 5. Undriven Damped Oscillations of Physical Pendulum. To achieve the steady-state quickly while still having enough data to detect an amplitude and period, the spacing of the magnets is set to $(25.22 \pm 0.05)mm$. This damps out the oscillations within 6 seconds. The ratio between amplitudes is used to measure the damping constant for this system, with which the resonant frequency will be predicted.

The damping constant is found using the following formula:

$$\tau = -\frac{T}{\ln\left(\frac{\theta(T+t)}{\theta(t)}\right)}$$

The period T is found by calculating the average period at each peak ($T_{avg} = \frac{t_n - t_1}{n-1}$). The best value was taken to be the mean of the three calculated values and the uncertainty $\delta T = \frac{STDEV.S(All\ values)}{\sqrt{3}}$, giving $T = (1.463 \pm 0.007)s$. With these we also determine that $\omega_{damped} = \frac{1}{T} = (0.684 \pm 0.003)\ s^{-1}$

The damping constant was then calculated for each the ratio $r = \frac{V(T+t)}{V(t)}$ using the above formula. The mean of these values is taken as τ_{best} and $\delta\tau = \frac{STDEV.S(All\ values)}{\sqrt{3}}$. This gives $\tau = (1.210 \pm 0.013)\ s$.

The resonant frequency can finally be predicted:

$$\omega_R = \sqrt{\omega_o^2 - 2\frac{1}{\tau^2}}$$

$$\omega_R = \sqrt{\left((0.7067 \pm 0.0014)\mathrm{s}^{-1}\right)^2 - \frac{2}{\left((1.210 \pm 0.013)\ s\right)^2}}$$

$$\omega_R^* = \sqrt{(0.4994 \pm 0.0019)s^{-2} - (1.366 \pm 0.028)s^{-2}}$$

$$\omega_R^{**} = \sqrt{(-0.867 \pm 0.028)s^{-2}}$$

*Uncertainty determined by $\delta(x^n) = |x_{best}^n||n|\left(\frac{\delta x}{|x|}\right)$ and $\delta(Ax) = |A|\delta x$

**Uncertainty determined by $\delta(x+y) = \sqrt{(\delta x)^2 + (\delta y)^2}$

An issue is run into with this prediction: the resonant frequency prediction is imaginary. If the damping constant is looked at closely, one would realize that $\tau = (1.210 \pm 0.013)\ s$ contradicts the definition that for this system to be underdamped $\tau > (1.415 \pm 0.003)s$. There is therefore an inconsistency in the data collected. This could be attributed to an unintended change in setup such as the rotation pulley's connection to the string, which in fact had to be adjusted during the measurement of the resonant frequency. While this discrepancy exists, the comparison of the Q factor, which is based on the measured resonant frequency and either damping constant or resonance width. If this is consistent, the properties of harmonic motion in a rigid body can still be confirmed.

The resonant frequency is then measured by adjusting the wave driver. Based on the assumption that $\omega_o \approx \omega_R$, the undamped frequency is used to begin looking for the resonant frequency. The Lissajous figures, which are parametric plots of the angle vs. voltage data, is used to determine the resonant frequency.

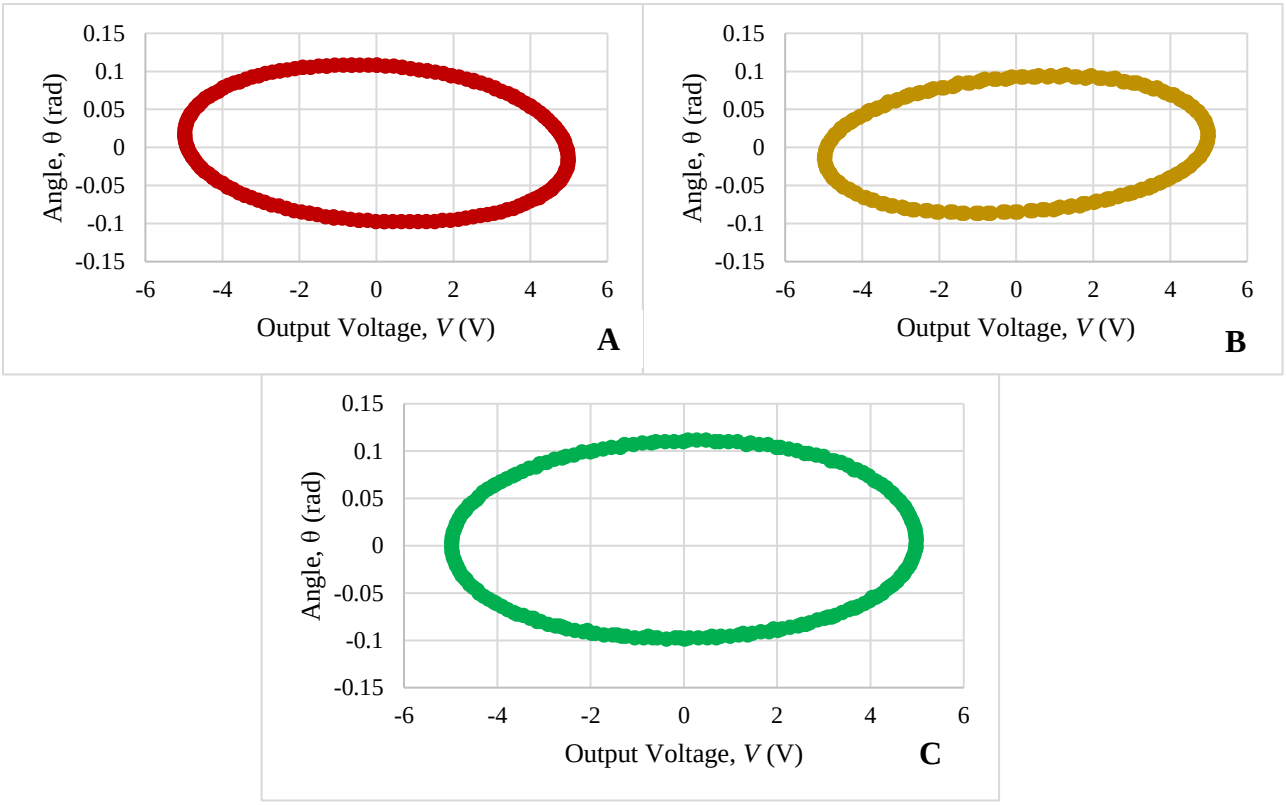

Figure 6. Determination of Resonant Frequency The resonant frequency is measured by plotting the Lissajous figure for the drive frequency used. Figure 5A (left) was produced by a drive frequency of 0.855 s^{-1}, Figure 5B (right) was produced by a drive frequency of 0.900 s^{-1}, and Figure 5C (bottom) was produced by 0.875 s^{-1}. As Figure 5C was the most symmetric plot found. The symmetry began to disappear about 0.025 s^{-1}. Therefore, the measured resonant frequency is $\omega_R = (0.875 \pm 0.025)s^{-1}$.

The quality factor for the system can now also be found using the definition $Q = \tau\pi\omega_R$

$$Q = \pi * (1.210\, s \pm 0.013s) * (0.875\mathrm{s}^{-1} \pm 0.025\mathrm{s}^{-1})$$

$$Q = \pi * (1.02 \pm 0.09) = 3.2 \pm 0.3$$

$$\delta Q = \pi * (1.210 * 0.875)\sqrt{\left(\frac{0.013}{1.210}\right)^2 + \left(\frac{0.025}{0.875}\right)^2}$$

Based on the above method, Q is measured to be 3.2 ± 0.2. Another method to calculate Q is to estimate it as the ratio of the resonant frequency to the resonance. We first examine the amplitude response of our pendulum, which plots the resulting amplitude of several driving frequencies.

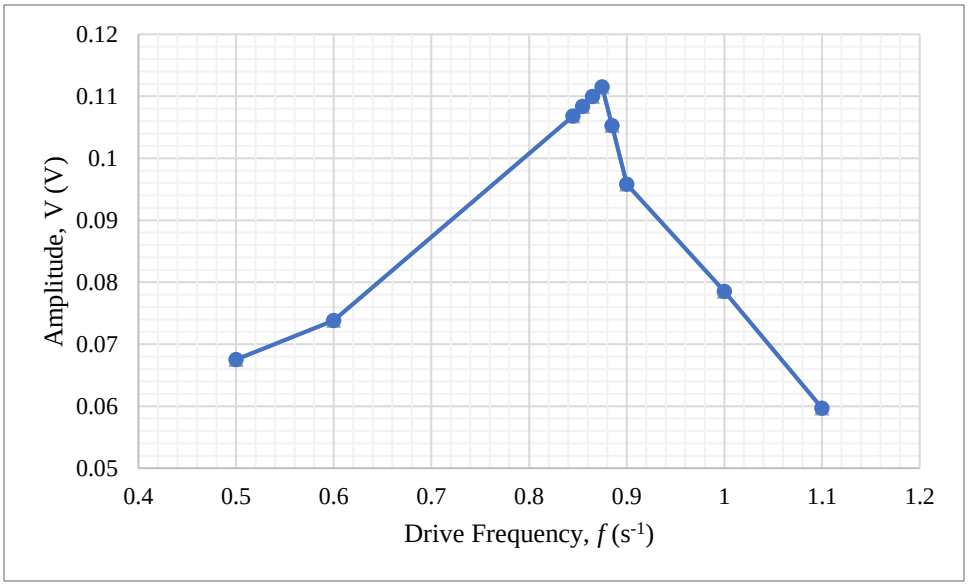

Figure 7. Amplitude Response of Damped Pendulum Oscillator. The resulting amplitude for several driving frequencies around the resonant frequency are taken. The amplitude was obtained by taking the mean of the maximum and minimum output voltage for each dataset. The Lorentzian shape is somewhat seen, but greater number of drive frequencies observed would have made the shape more defined.

To find the resonance width $\Delta\omega$, the frequencies that would produce the $\frac{1}{\sqrt{2}}$ of the height are predicted using the graph. Since the maximum amplitude is 0.1115 V, the frequencies estimated to produce an amplitude of $\frac{1}{\sqrt{2}} * 0.1115\ \text{V} = 0.0789\ \text{V}$ are $(0.65 \pm 0.06)\ s^{-1}$ and $(0.99 \pm 0.03) s^{-1}$. The uncertainty is estimated by the proximity to a measured point and by the lack of points leading to a less defined curve. Therefore, $\Delta\omega = (0.34 \pm 0.09)\ s^{-1}$. Now, Q is calculated to be

$$Q \approx \frac{\omega_o}{\Delta\omega} \approx \frac{(0.7067 \pm 0.0014)s^{-1}}{(0.34 \pm 0.09)s^{-1}} = 2.1 \pm 0.4$$

$$\delta Q = \left(\frac{0.7067}{0.34}\right)\sqrt{\left(\frac{.0014}{.7067}\right)^2 + \left(\frac{0.09}{0.34}\right)^2}$$

Based on the second method, $Q = 2.1 \pm 0.4$. This is not consistent with $Q = 3.2 \pm 0.3$ calculated from the first method as the bounds for each value do not overlap. This could be due not calculating uncertainty correctly or the fact that the undamped frequency is inconsistent with this set up as seen earlier. In addition, the latter method yields a 19.0% uncertainty, which is quite high. Therefore, the first method is a little more reliable in terms of getting a more precise result for the setup. The uncertainty of the second method could also be reduced by increasing the number of points; to drastically change the error however, the number of points needed to define the resonance curve more accurately is not quite efficient.

Yet another method can be used to approximate Q. The frequencies that yield $\frac{1}{\sqrt{2}} * 0.1115\ \text{V} = 0.0789\ \text{V}$ were then experimentally determined to be $(0.675 \pm 0.003)s^{-1}$ and $(1.000 \pm 0.003)s^{-1}$, yielding a measured width of $\Delta\omega = (0.325 \pm 0.004)s^{-1}$

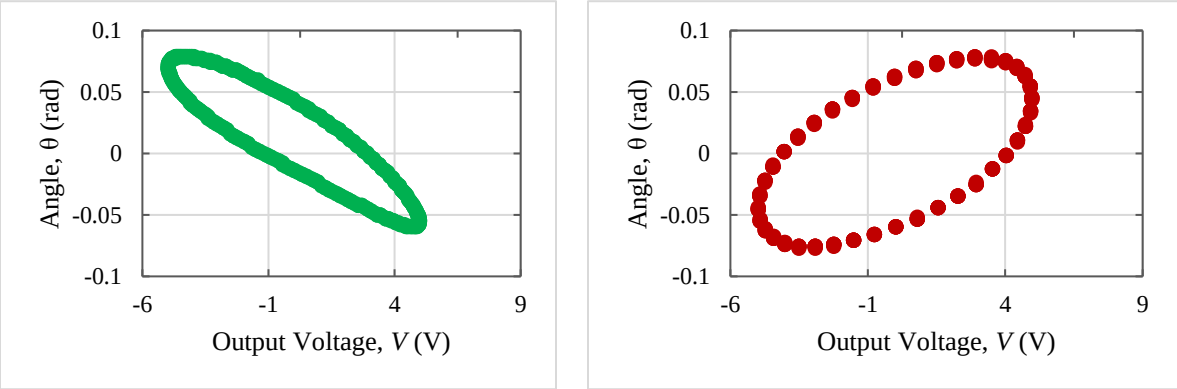

Figure 8. Lissajous Figures for the Resonance Width Bounds. The left is the produced figure for $(0.675 \pm 0.003)s^{-1}$ and right is the produced figure for $(1.000 \pm 0.003)s^{-1}$. Both figures have a maximum at $\approx 0.0789\ V$ and have a tilt with a slope of similar magnitudes. With respect to the "left" narrow edge of the figures, the lower frequency is tilted upwards and the higher frequency is tilted downwards.

Q can also be approximated by $Q \approx \frac{\omega_R}{\Delta\omega}$. This gives

$$Q \approx \frac{\omega_R}{\Delta\omega} \approx \frac{(0.875 \pm 0.025)\text{s}^{-1}}{(0.325 \pm 0.004)s^{-1}} = 2.73 \pm 0.18$$

$$\delta Q = \left(\frac{0.875}{0.325}\right)\sqrt{\left(\frac{.025}{.875}\right)^2 + \left(\frac{0.004}{0.325}\right)^2}$$

The calculated value of Q =2.73 $\pm$ 0.18 just overlaps with the first calculated value of $Q = 3.2 \pm 0.3$. It almost overlaps with the second value as well, with the second higher limit and the third lower limit being 0.05 away. This last method is most accurate as while the other calculations have a lot of indirect measurements, increasing uncertainty, this one is obtained from three raw values of data. It also is very precise is relation to the other Q values; therefore, it is most likely the closest value to the real quality factor.

Waves on a Vibrating String

Now the focus is shifted to the harmonic motion of a vibrating string, which is a spatially extensive body.

Part 1: Wave Speed

First the properties of travelling wave speed are investigated. The tension T and linear mass density μ of the string are measured to predict the wave speed using the formula

$$v = \sqrt{\frac{T}{\mu}}$$

Since the hanging mass affects the tension and linear mass density of the string a series of calculations are performed on the measurements taken to find these two values. The mass used is first calculated to complete the table below.

Total Mass of String: $(0.01500 \pm 0.00005)kg$
Total Length of Relaxed String: $(2.255 \pm 0.001)m$
Length of Excess String: $(0.255 \pm 0.001)m$
Mass of Used String = $\frac{(2.255 \pm 0.001) - (0.255 \pm 0.001)}{(2.255 \pm 0.001)} * (0.015 \pm 0.00005)kg$
Mass Used $m_s = (0.013 \pm 0.001)kg$

Trial	Formula	1	2	2
Tensed String Length L_s (m)	Measured	1.867 ± 0.001	1.915 ± 0.001	1.918 ± 0.001
Linear Mass Density μ (kg/m)	$\frac{m_s}{L_s}$	0.00713 ± 0.00005	0.00694 ± 0.00005	0.00694 ± 0.00005
Hanging String Length L_h (m)	Measured	0.658 ± 0.001	0.665 ± 0.001	0.745 ± 0.001
Hanging String Mass m_h (kg)	$\mu * L_h$	0.00469 ± 0.00003	0.00461 ± 0.00002	0.00517 ± 0.00003
Hanging Weight Mass m_w (kg)	Measured	0.04970 ± 0.00005	0.1995 ± 0.0001	0.3998 ± 0.0002
Tension T (N)	$(m_h + m_w)g$	0.5330 ± 0.0006	2.000 ± 0.001	3.959 ± 0.001

Table 1. Determination of String Properties and Measurements The tension and linear mass was calculated while the measurements were being taken in Excel. This table compactly shows this step. The tension and linear mass density will be restated for each trial's analysis.
The uncertainties for each calculation was derived from the following:

- $\delta m_s \approx \left|\frac{2.000}{2.255}\right| \sqrt{\left(\frac{0.001}{2.000}\right)^2 + \left(\frac{0.001}{2.255}\right)^2}$
- $\delta \mu = \left|\frac{m_{s_{best}}}{L_{s_{best}}}\right| \sqrt{\left(\frac{\delta m_s}{m_{s_{best}}}\right)^2 + \left(\frac{\delta L_s}{L_{s_{best}}}\right)^2}$
- $\delta m_h = \left|\mu_{best} * L_{h_{best}}\right| \sqrt{\left(\frac{\delta \mu}{\mu_{best}}\right)^2 + \left(\frac{\delta L_h}{L_{h_{best}}}\right)^2}$
- $\delta T = g * \sqrt{(\delta m_h)^2 + (\delta m_w)^2}$

Trial 1

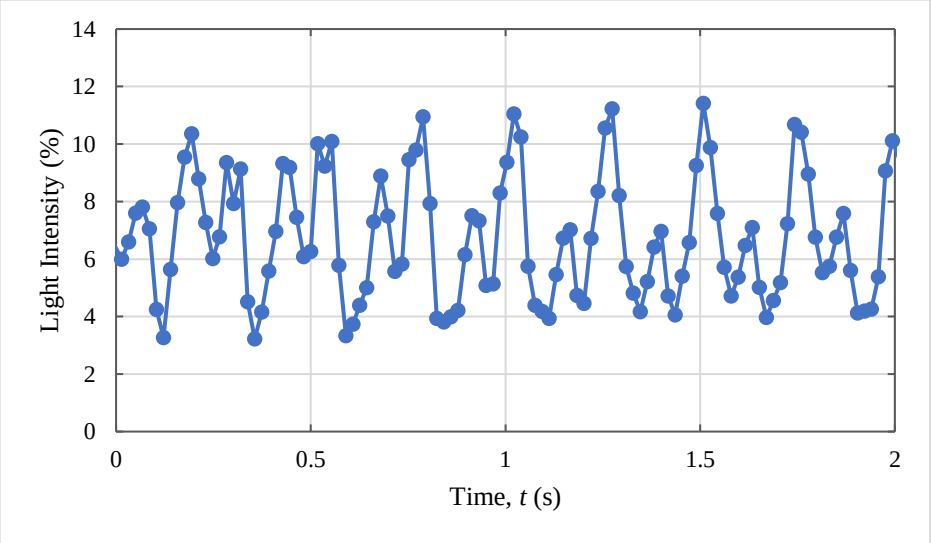

Figure 9. Determining Speed of Travelling Wave for Mass 1. A weight with mass $(49.70 \pm 0.05)g$ hung off the string over a pulley. When the wave driver is turned on, travelling waves are created by vibrating the string. The laser beam spot thus scattered into the photodiode producing the signal above. A clear repeating figure can be seen, confirming the expected wave behavior. An offset was subtracted from the time data to have it center at $t = 0\ s$ The time delay was estimated using the average Δt between the 13 peaks of the signal. $\delta t_d = \left(\frac{STDEV.S(All\Delta t)}{\sqrt{12}}\right)$. Therefore $t_d = (0.238 \pm 0.004)s$.

The predicted speed, using the determined values $T = (0.5330 \pm 0.0006)N$ and $\mu = (0.00713 \pm 0.00005)\ kg/m$ is

$$v_p = \sqrt{\frac{(0.5330 \pm 0.0006)kg * \left(\frac{m}{s^2}\right)}{(0.00713 \pm 0.00005)\ kg/m}} = (8.65 \pm 0.03)\ m/s$$

The following was derived for the uncertainty and for Trials 2 and 3 as well.

$$\delta v_p = \frac{1}{2} * \sqrt{\frac{T_{best}}{\mu_{best}}} * \sqrt{\left(\frac{\delta T}{T_{best}}\right)^2 + \left(\frac{\delta \mu}{\mu_{best}}\right)^2}$$

The experimental speed is then calculated. The wavelength is estimated using twice the distance between the pulley and clip clamp, yielding $d = (2.418 \pm 0.002)m$. As per Figure 9, $t_d = (0.119 \pm 004)$s

$$v_m = \frac{d}{t_d} = \frac{(2.418 \pm 0.002)m}{(0.238 \pm 0.004)\text{s}} = (10.16 \pm 0.17)\ m/s$$

$$\delta v_d = \left|\frac{d}{t_d}\right| * \sqrt{\left(\frac{\delta d}{d_{best}}\right)^2 + \left(\frac{\delta t_d}{t_{d\,best}}\right)^2}$$

For trial 1, $v_m = (10.16 \pm 0.17)\ m/s$ does not agree with $v_p = (8.65 \pm 0.03)\ m/s$

Trial 2

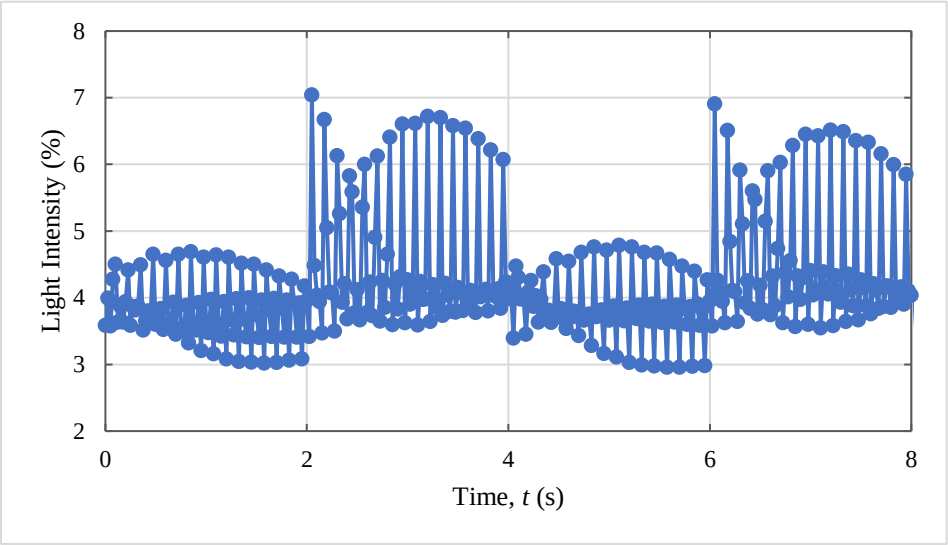

Figure 10. Determining Speed of Travelling Wave for Mass 2. For trial 2, a weight with mass $(199.5 \pm 0.1)g$ hung from the string. While a larger time domain is needed compared to Trial 1, a clear repeating figure can be seen, confirming the expected wave behavior. An offset was subtracted from the time data to have it center at $t = 0\ s$ The time delay was estimated using the average Δt between the 13 peaks of the signal. $\delta t_d = \left(\frac{STDEV.S(All\Delta t)}{\sqrt{12}}\right)$. Therefore $t_d = (0.1271 \pm 0.0021)s$.

The predicted speed, using the determined values $T = (2.000 \pm 0.001)N$ and $\mu = (0.00694 \pm 0.00005)\ kg/m$ is

$$v_p = \sqrt{\frac{(2.000 \pm 0.001)kg * \left(\frac{m}{s^2}\right)}{(0.00694 \pm 0.00005)\ kg/m}} = (16.97 \pm 0.06)\ m/s$$

The experimental speed is then calculated. As mentioned earlier, the constant distance is $d = (2.418 \pm 0.002)m$. As per Figure 10, $\mathrm{t_d} = (0.1271 \pm 0.0021)\mathrm{s}$

$$v_m = \frac{d}{t_d} = \frac{(2.418 \pm 0.002)m}{(0.1271 \pm 0.0021)\mathrm{s}} = (19.0 \pm 0.3)\ m/s$$

For trial 2, $v_m = (19.0 \pm 0.3)\ m/s$ is inconsistent with $v_p = (16.97 \pm 0.06)\ m/s$. However, the increased tension led to a higher speed.

Trial 3

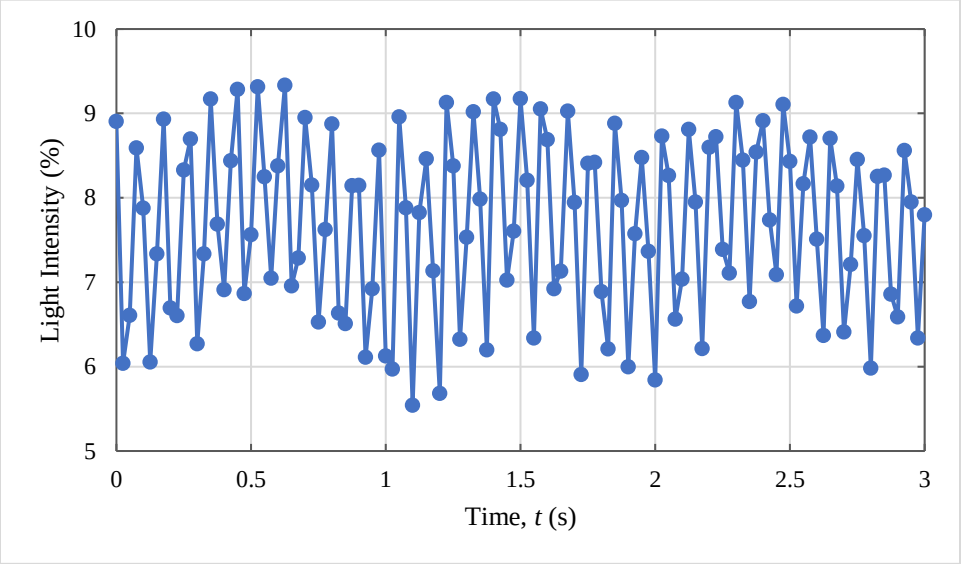

Figure 11. Determining Speed of Travelling Wave for Mass 3. For trial 3, a weight with mass $(398.8 \pm 0.2)g$ hung from the string. A three second time duration shows a clear repeating figure, confirming the expected wave behavior. An offset was subtracted from the time data to have it center at $t = 0\ s$. The time delay was estimated using the average Δt between the 13 peaks of the signal. $\delta t_d = \left(\frac{STDEV.S(All\Delta t)}{\sqrt{12}}\right)$. Therefore $t_d = (0.088 \pm 0.004)s$

The predicted speed, using the determined values $T = (3.959 \pm 0.001)N$ and $\mu = (0.00694 \pm 0.00005)\ kg/m$ is

$$v_p = \sqrt{\frac{(3.959 \pm 0.001)kg * \left(\frac{m}{s^2}\right)}{(0.00694 \pm 0.00005)\ kg/m}} = (23.88 \pm 0.13)\ m/s$$

The experimental speed is then calculated. As per Figure 11, $\mathrm{t_d} = (0.088 \pm 0.004)\mathrm{s}$

$$v_m = \frac{d}{t_d} = \frac{(2.418 \pm 0.002)m}{(0.088 \pm 0.004)\mathrm{s}} = (27 \pm 1)\ m/s$$

For trial 3, $v_m = (27 \pm 1)\ m/s$ is inconsistent with $v_p = (23.88 \pm 0.13)\ m/s$.

For all three trials, the measured and predicted speed are inconsistent, and $v_m > v_p$. This could be due to an inaccurate measurement of the lengths and miscalculation of uncertainty. Even so, it was still observed that increasing tension increases the speed, thus confirming the conceptual relationship between v and T.

Part 2: Standing Waves

To predict the frequency for each mode of a standing wave, the following function is used

$$f(n) = n\left(\frac{v}{2L}\right)$$

The set up used for the string is that from Trial 3 of the previous section, therefore the speed is $v = (27 \pm 1)m/s$.

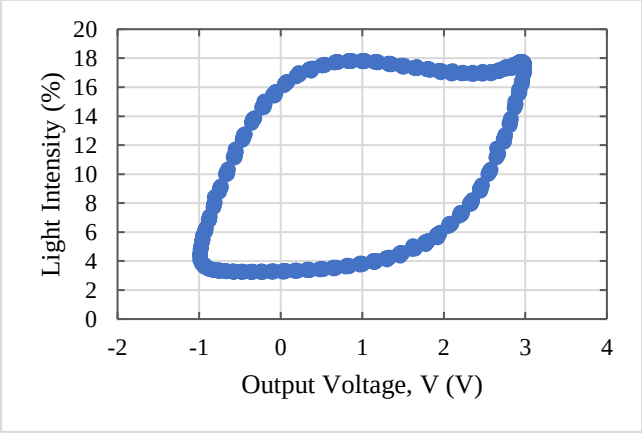

Figure 12. Lissajous Figure for n =1 mode

The fundamental frequency is predicted to be $f_1 = \frac{(27\pm1)\ m/s}{(2.418\pm0.002)s} = (11.2 \pm 0.4)s^{-1}$

Using maximum amplitude: $f_{1_{max}} = (12.3 \pm 0.2)s^{-1}$

Measured (Lissajous figures): $(10.67 \pm 0.05)s^{-1}$

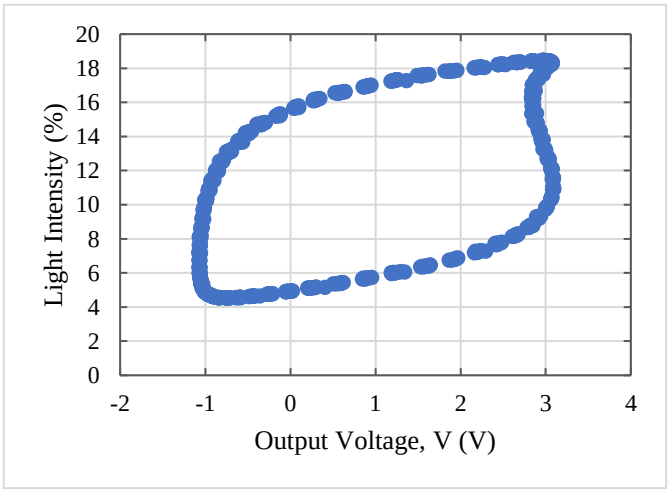

Figure 13. Lissajous Figure for n = 2 mode

The 2nd harmonic is predicted to be $f_2 = \frac{2*(27\pm1)\ m/s}{(2.418\pm0.002)s} = (22.4 \pm 0.8)s^{-1}$

Using fundamental frequency: $f_{2_{fund}} = 2 * (10.67 \pm 0.05)s^{-1} = (21.3 \pm 0.1)\ s^{-1}$

Measured (Lissajous figures): $(21.3 \pm 0.2)\ s^{-1}$

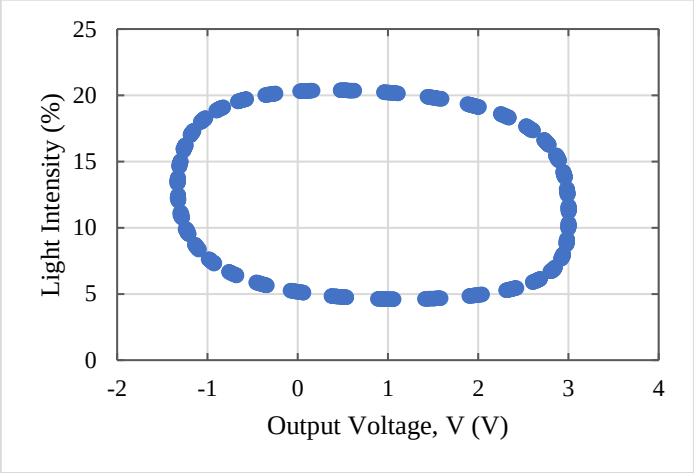

Figure 14. Lissajous Figure for n = 4 mode

The 4th harmonic should theoretically be $f_4 = \frac{4*(27\pm1)\ m/s}{(2.418\pm0.002)s} = (45 \pm 1)s^{-1}$

Using fundamental frequency: $f_{4_{fund}} = 4 * (10.67 \pm 0.05)s^{-1} = (42.7 \pm 0.2)s^{-1}$

Measured (Lissajous figures): $(46.71 \pm 0.05)s^{-1}$

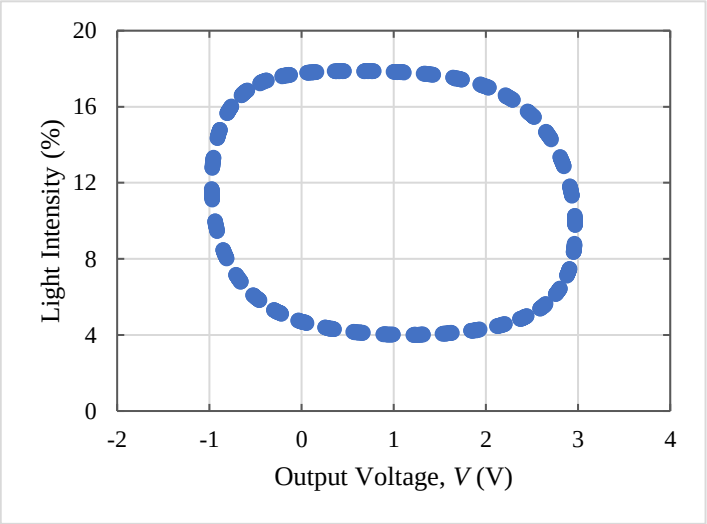

Figure 15. Lissajous Figure for n = 6 mode

The 6th harmonic should theoretically be $f_6 = \frac{6*(27\pm1)\ m/s}{(2.418\pm0.002)s} = (67 \pm 2)s^{-1}$

Using fundamental frequency: $f_{6_{fund}} = 6 * (10.67 \pm 0.05)s^{-1} = \ (64.0 \pm 0.3)s^{-1}$

Measured (Lissajous figures): $(68 \pm 1)s^{-1}$

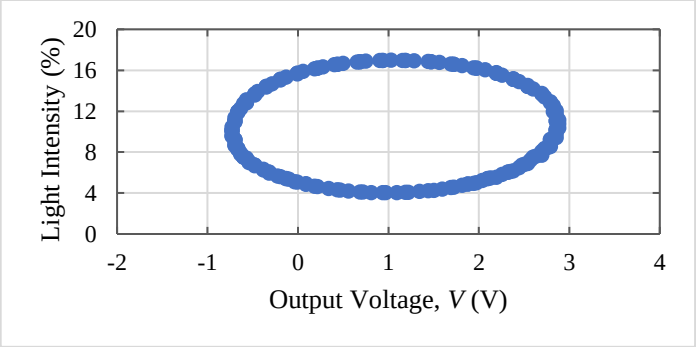

Figure 16. Lissajous Figure for n = 8 mode

The 8th harmonic should theoretically be $f_8 = \frac{8*(27\pm1)\ m/s}{(2.418\pm0.002)s} = (90 \pm 3)s^{-1}$

Using fundamental frequency: $f_{8_{fund}} = 8 * (10.67 \pm 0.05)s^{-1} = (85.4 \pm 0.4)s^{-1}$

Measured (Lissajous figures): $(88 \pm 1)s^{-1}$

Lissajous Figure for n = 30 mode

The 30th harmonic should theoretically be $f_{30} = \frac{30*(27\pm1)\ m/s}{(2.418\pm0.002)s} = (336 \pm 12)s^{-1}$

Using fundamental frequency: $f_{30_{fund}} = 30 * (10.67 \pm 0.05)s^{-1}\ (320 \pm 2)s^{-1}$

Measured (Lissajous figures): $COULD\ NOT\ BE\ FOUND$. The signal was too noisy, most likely because the vibrations are too small.

As the modes got higher, the error increased and the prediction using the fundamental frequency became inconsistent with the measured values. The values were in fact more consistent with the theoretical values based on the wave speed. This indicates that the measured fundamental frequency may have been miscalculated or not all uncertainty was accounted for.

Part 3: Boundary Effects

To study the effects of intermediary boundary conditions, the middle node was constrained with a rod and finger for n= 2, 4, and 4. Below compares the graphs with and without this constraint. The "amplitude" is approximated by peak-to-peak size of signal due to being proportional to it.

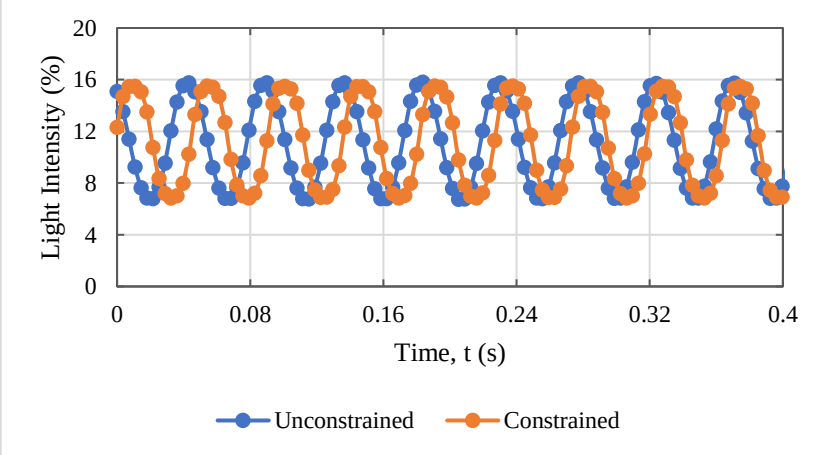

Figure 17. Effect of Constraint in n=2 mode. The amplitude before the constraint is found by taking the average peak-to-peak size, which is $A = (0.0468 \pm 0.0022)\%$. After the constraint, the amplitude is $A = (0.0452 \pm 0.0017)\%$. This shows very little effect by the constraint.

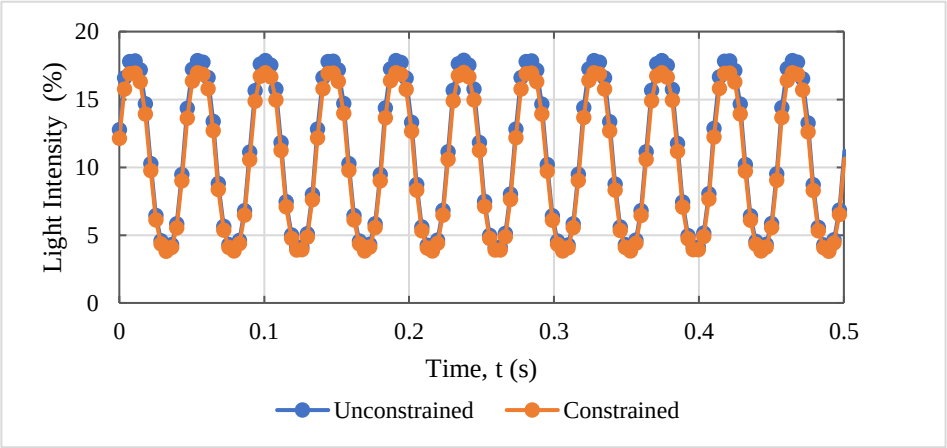

Figure 18. Effect of Constraint in n=4 mode. The amplitude before the constraint is found by taking the average peak-to-peak size, which is $A = (0.0468 \pm 0.0022)\%$. After the constraint, the amplitude is $A = (0.0452 \pm 0.0011)\%$. This shows very little effect by the constraint.

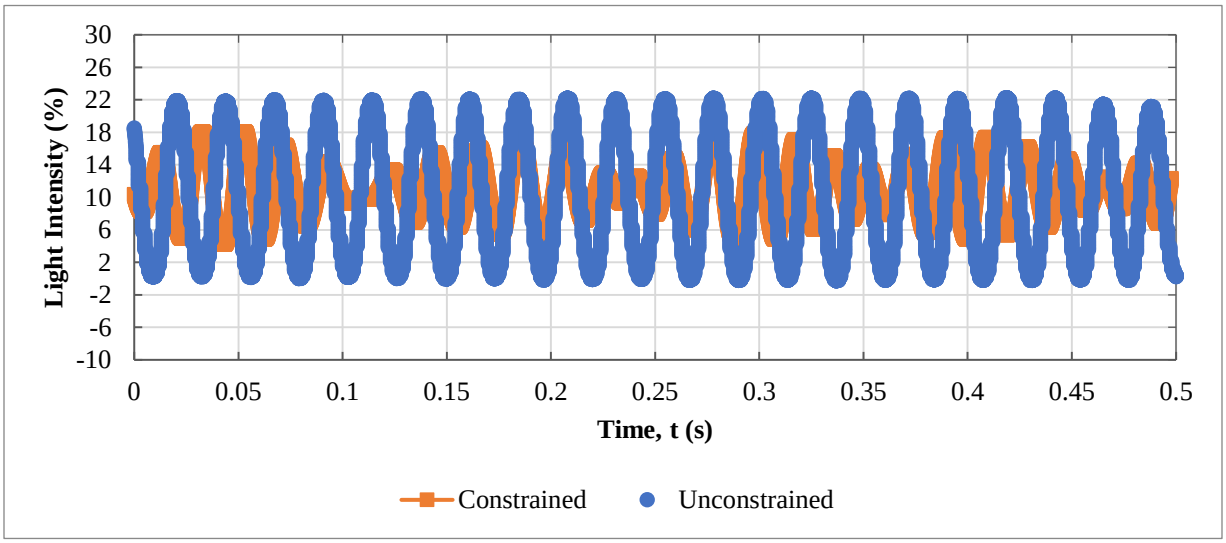

Figure 19. Effect of Constraint in n=5 mode. The amplitude before the constraint is found by taking the average peak-to-peak size, which is $A = (0.023 \pm 0.003)\%$. After the constraint, the amplitude is $A = (0.015 \pm 0.002)\%$. This shows a drastic effect by the constraint. The difference between this mode from n= 2 and 4 is that it has no node exactly in the middle. Such a condition hence prevents modes with no middle node from producing normal waves.

CONCLUSIONS

The purpose of this experiment was to study harmonic motion in the oscillations of a rigid, physical pendulum and in the vibrations of a spatially extensive string.

For the aluminum pendulum, the three damping regimes were observed by adjusting the magnet spacing through which the pendulum oscillated. The critically damped oscillation was

found at (14.1 ± 0.3)mm. The undamped frequency was found to be $\omega_o = (0.7067 \pm 0.0014)\mathrm{s}^{-1}$, therefore determining that the damping constant of a system must greater than $\tau_{critical} = (1.415 \pm 0.003)s$ to exhibit underdamped oscillation. This was contradicted when for the undriven underdamped oscillations, $\tau = (1.210 \pm 0.013)\ s$. This could have occurred due to an unintended change in the setup and torque of the pendulum, along with not calculating enough uncertainty. While a resonant frequency could not be predicted, it was measured using Lissajous figures to be $\omega_\mathrm{R} = (0.875 \pm 0.025)\mathrm{s}^{-1}$. Q was also calculated using three methods. The first used ω_R and τ to yield $Q = 3.2 \pm 0.3$.The second used the ratio of $\omega_o$to the estimated resonance width of the amplitude response to yield $Q = 2.1 \pm 0.4$. The last calculated the ratio of ω_R to the experimentally measured resonance width to get Q =2.73 $\pm$ 0.18; this was determined to be most accurate due to involving only direct measurements and being nearly consistent with the other two Q values, which disagree with each other.

For the vibrating string, the velocities of the travelling waves were measured using the string's determined tension and linear mass density, which varied with mass. The predicted velocities were all inconsistent and less than the measured velocities (for example, $(8.65 \pm 0.03)\ m/s < (10.16 \pm 0.17)\ m/s$), but a positive correlation between the tension and speed was still evident. The error could be due to inaccurate measurements for length, which were taken with a rigid meter stick. An improvement would be to use measuring tape instead, or replacing the pulley with a sharp corner instead. Next, the Lissajous figures were again used to determine that the fundamental frequency for the system's standing waves is $f_1 = (10.67 \pm 0.05)s^{-1}$. This value is used to efficiently predict and measure the successive harmonics. Unfortunately, the 30$^{\text{th}}$ harmonic could not be found as the vibrations were most likely too small; this could have been improved with using an even higher amplitude or a string shorter length. The further examination of the boundary constraint effects on n= 2, 4, and 5 showed that while n=2 and n=4 experienced very little change, the amplitude 5$^{\text{th}}$ harmonic was noticeably compromised by the constraint due to not having a node at that position.